THE JOURNAL OF PHYSICAL CHEMISTRY Letters

Letter

pubs.acs.org/JPCL

Ultrabroad Photoluminescence and Electroluminescence at New Wavelengths from Doped Organometal Halide Perovskites

Yang Zhou,[†] Zi-Jun Yong,[†] Kai-Cheng Zhang,[†] Bo-Mei Liu,[†] Zhao-Wei Wang,[†] Jing-Shan Hou,[‡] Yong-Zheng Fang,[‡] Yi Zhou,[†] Hong-Tao Sun,*[,†] and Bo Song*[,†]

[†]College of Chemistry, Chemical Engineering and Materials Science, Soochow University, Suzhou 215123, China

[‡]School of Materials Science and Engineering, Shanghai Institute of Technology, Shanghai 201418, China

Supporting Information

ABSTRACT: Doping of semiconductors by introducing foreign atoms enables their widespread applications in microelectronics and optoelectronics. We show that this strategy can be applied to direct bandgap lead-halide perovskites, leading to the realization of ultrawide photoluminescence (PL) at new wavelengths enabled by doping bismuth (Bi) into lead-halide perovskites. Structural and photophysical characterization reveals that the PL stems from one class of Bi doping-induced optically active center, which is attributed to distorted [PbI_6] units coupled with spatially localized bipolarons. Additionally, we find that compositional engineering of these semiconductors can be employed as an additional way to rationally tune the PL properties of doped perovskites. Finally, we accomplished the electroluminescence at cryogenic temperatures by using this system as an emissive layer, marking the first electrically driven devices using Bi-doped photonic materials. Our results suggest that low-cost, earth-abundant, solution-processable Bi-doped perovskite semiconductors could be promising candidate materials for developing optical sources operating at new wavelengths.

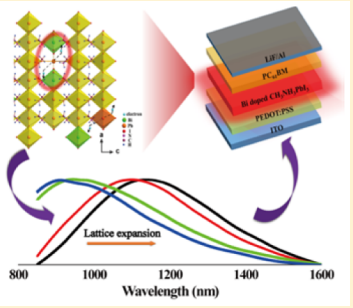

Over the past several years, solution-processable metal halide perovskite semiconductors, in particular the hybrid organic−inorganic lead halide perovskites, have shown huge potential in the field of optoelectronic devices including solar cells,[1−15] light-emitting diodes (LEDs),[16−21] lasers,[22−25] laser cooling,[26] and photodetectors.[27,28] This mainly has been spurred by their low-cost solution processability and outstanding intrinsic optoelectronic properties (e.g., large absorption coefficients, long carrier lifetimes, tunable band gaps, and high luminescence quantum yields). As light absorber layers, $MAPbX_3$ (where MA = methylammonium and X = Cl, Br, or I or mixtures thereof) semiconductors have enabled inexpensive solar cells with certified power conversion efficiencies of up to 22.1%.[7] After revolutionizing the field of photovoltaics, direct bandgap lead halide perovskites are also emerging as emissive components because of narrow-band emissions with high photoluminescence (PL) quantum efficiencies (QEs).[16−31] Up till now, optically pumped lasing and room-temperature EL devices based on this class of systems have been successfully demonstrated, promising a bright future for low-cost and solution-processed optically pumped or even electrically driven laser devices.[32] However, despite these intriguing advances, pristine lead halide perovskites are not capable of luminescing or lasing at wavelengths longer than 1.0 μm owing to their relatively large bandgaps, although quantum-dot-in-perovskite solids could show such emissions.[33−35] In lead halide perovskites, MA and Pb cations are surrounded by 12 and 6 halide anions, respectively, thus making it a superb candidate to accommodate a variety of foreign ions with similar ionic radii to that of MA or Pb.

Doping of semiconductors, a process of intentional insertion of impurity atoms into an extremely pure crystal, was introduced in the 1940s and is the basis for the widespread applications of semiconductors in microelectronics and optoelectronics.[36] In general, doping a semiconductor introduces new energy states within the band gap, allowing for the occurrence of low-energy electronic transitions. It is noteworthy that previous works have merely focused on the investigation of pristine metal halide perovskites and their related devices. As far as we are aware, doping of perovskites, aiming at attaining emerging optoelectronic features, has not received extensive attention in this community.

Herein, we demonstrate that $MAPbI_3$ films can show ultrawide NIR PL in the range of 850−1600 nm that is achieved by simply doping bismuth, a versatile element existing in an array of functional materials.[37−41] Interestingly, the incorporation as well as the activation of NIR active centers in the perovskite matrix can be readily accomplished by spin-coating a dimethylformamide (DMF) solution containing BiI_3, CH_3NH_3I, and PbI_2, followed by low-temperature treatment under a nitrogen atmospheric condition. The photophysical properties of the resulting films can be tuned by tailoring the fabrication parameters. Combined experimental evidence obtained from PL, X-ray photoelectron spectroscopy (XPS), and electron spin resonance (ESR) leads us to attribute the observed ultrawide PL to the electronic transition of the

Received: May 26, 2016
Accepted: July 5, 2016
Published: July 5, 2016

DOI: 10.1021/acs.jpclett.6b01147
J. Phys. Chem. Lett. 2016, 7, 2735−2741

luminescent center created by Bi incorporation. Interestingly, we find that compositional engineering of lead halide perovskites, a strategy widely used for their bandgap tuning, can be employed as an additional way to tune the photophysical properties of doped systems, leading to tunable PL emissions in a broad spectral range. Finally, we also demonstrate the NIR LEDs operating at new wavelengths by using this emerging system.

The Bi-doped $MAPbI_3$ were prepared by spin-coating the precursor solution, followed by annealing on a hot plate at 100 °C to obtain uniform films. The sample is denoted as x% (i.e., the molar ratio of Bi to Pb). As confirmed by X-ray diffraction (XRD), the crystallinity of the $MAPbI_3$ films does not show noticeable change after incorporating a small amount of Bi (Figure S1, Supporting Information), and no impurity phases assigned to BiI_3 or Bi-related byproducts can be detected, suggesting that Bi ions are incorporated into the perovskite matrix. As a direct bandgap semiconductor, the $MAPbI_3$ film demonstrates strong PL band centered at 782 nm (Figure 1a).

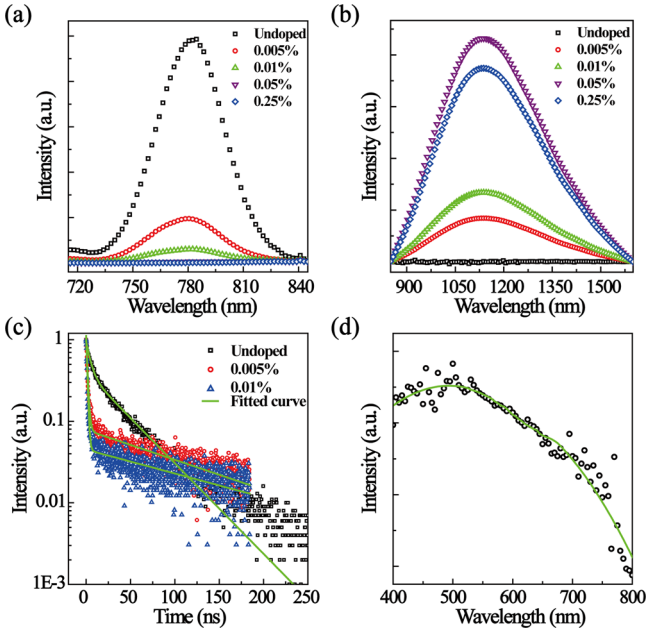

Figure 1. Photophysical properties of the pristine and Bi-doped $MAPbI_3$ films. (a, b) PL spectra of the pristine and Bi-doped $MAPbI_3$ films under the excitation of 517 nm. The spectral response of the detection system was corrected. (c) Decay curves of the pristine and Bi-doped $MAPbI_3$ films monitored at 782 nm. (d) Typical PL excitation spectrum of the 0.01% film monitored at 1150 nm. The solid line was drawn to guide the eye.

Interestingly, the intensity of this band monotonously decreases with the increase of Bi concentration, along with the occurrence of one ultrawide emission band peaked at ca. 1140 nm (Figure 1b). The full width at half-maximum (fwhm) of this new band is as large as 380 nm, almost covering the whole telecommunication windows of O (1260−1360 nm), E (1360−1460 nm), S (1460−1530 nm) bands, and even C (1530−1565 nm) and L (1565−1625 nm) bands. Hereafter, this ultrawide emission band is termed as "telecom emission". To achieve the strongest telecom emission from these films, we next investigated the impact of preparation parameters on NIR PL properties, with particular focuses on Bi doping concentration, annealing temperature, as well as annealing duration. We find that the 0.05% sample displays the strongest emission when annealed at 100 °C for 1 min (Figure S2). It is necessary to point out that the $MAPbI_3$ film without Bi does not show any PL in the telecommunication windows. This suggests that the telecom emission in doped films originates from bismuth-related active centers (BRACs). Although the preparation parameters greatly influence the emission intensity, the PL lineshapes are almost identical for different samples (Figure S3). Additionally, the emission lineshapes are independent of the excitation wavelengths, giving a clear indication that the telecom emission stems from the same class of BRACs (Figure S4). This is in stark contrast to other Bi-doped systems that usually demonstrate excitation-wavelength-dependent NIR emission profiles owing to the coexistence of multitype active centers.[38] We further measured the internal QEs of the telecom emission for two representative films under the excitation of 730 nm light with a power of ca. 10 mW, which are 0.03% and 0.035% for the 0.005% and 0.05% films, respectively.

More insight into the peculiar luminescence properties of these films comes from time-resolved PL measurements. The decay of the pristine perovskites at 782 nm is slightly biexponential with a fast component of about 4.7 ns and a slower one of about 39.1 ns. As the increase of Bi concentration, the fast decays become dominant and much faster, followed by slower ones (Figure 1c, and Table S1 in Supporting Information), implying that Bi incorporation greatly alter the deexcitation channels of the carriers. Figure 1d displays the PL excitation spectrum of the 0.01% film monitored at 1150 nm. Obviously, the film can be efficiently photoexcited in a broad spectral range that can be extended to ca. 780 nm, corresponding to the bandgap energy of the $MAPbI_3$. The combined evidence from Figure 1c and d strongly suggests that the BRACs can be photoexcited via energy transfer from the semiconductor matrix to the BRACs.

Previous results have revealed that a sharp phase transition for the $MAPbI_3$ crystal occurs between 163 and 164 K, evidenced by the appearance of new reflections that violate the body-centering condition.[42,43] To evaluate the influence of the phase transition on the PL properties, we next carried out the PL measurement as a function of temperature (Figure 2a). Clearly, the PL from the 0.05% film increases as the decrease of the temperature from room temperature to 100 K. Interestingly, the PL is nearly identical for the tetragonal $I4/mcm$ and orthorhombic phases (Figure S5),[42,43] strongly indicating that the BRACs cannot be greatly affected by such a structural transformation. It is also noted that the decrease of the temperature redshifts the emission peak from ca. 1140 nm to ca. 1280 nm. In addition, it is found that the PL at 84 K is over 2 orders of magnitude stronger than that taken at room temperature. This suggests an internal QE of ca. 4.4% at 84 K for the 0.05% film, as a consequence of the inhibited nonradiative channels. To gain more information on the photophysical properties of Bi-doped $MAPbI_3$, the optical absorption spectra were taken (Figure 2b). The pristine $MAPbI_3$ shows a sharp optical absorption edge at 1.59 eV. Upon Bi incorporation, although the edge demonstrates a slight red shift, the systems preserve the direct bandgap feature well. It is necessary to note that no new absorption bands that could be assigned to the BRACs appear, caused by the small absorption coefficient of the BRACs relative to that of the $MAPbI_3$.

As one of the most thoroughly investigated main group elements, Bi has been regarded as "the wonder metal" because

DOI: 10.1021/acs.jpclett.6b01147
J. Phys. Chem. Lett. 2016, 7, 2735−2741

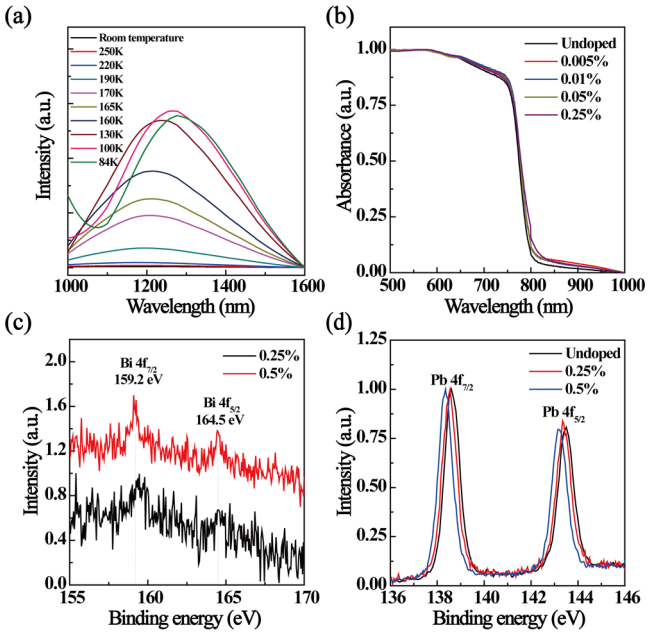

Figure 2. (a) Temperature-dependent NIR PL for the 0.05% film under the excitation of 517 nm. The signal at shorter wavelengths for the PL at 84 K may be from structural defects. (b) Absorption spectra of the pristine and Bi-doped $MAPbI_3$ films. (c) XPS spectra of Bi($4f_{5/2}$, $4f_{7/2}$) for the 0.25% and 0.5% films. (d) XPS spectra of Pb($4f_{5/2}$, $4f_{7/2}$) for the pristine, 0.25% and 0.5% films.

of its diverse oxidation states and profound propensities to form clusters. This distinct feature makes it behave as a broad range of optically active centers with peculiar emissions ranging from ultraviolet−visible to infrared.[38−41] To know the oxidation state of Bi in the perovskite films studied, we took the XPS spectra for the 0.5% and 0.25% samples. As shown in Figure 2c, for both samples the binding energies of the $4f_{7/2}$ and $4f_{5/2}$ levels of Bi are located at 159.1 and 164.4 eV, respectively, giving rise to the spin−orbit splitting of the core levels of 5.3 eV. This is indicative that Bi element exists as +3 in these perovskite films, which possesses an electron configuration of $(Xe)4f^{14}5d^{10}6s^2$. Additionally, the absence of any detectable signal in the ESR spectra indicates that the paramagnetic ions (e.g., Bi^{2+} and Bi^{+}) or defect centers do not exist in the samples or their concentrations is negligibly small (Figure S6). In light of the XPS and ESR analyses, coupled with the fact that Bi^{3+} is PL inactive in the NIR,[38−41] we conclude that not Bi^{3+} ions but other classes of active centers contribute to the observed NIR PL.

As is known, the stability and distortion of the perovskite ABX_3 structure depend on the ratio of the (A−X) distance to the (B−X) distance, called the tolerance factor, which is defined as

$$t = \frac{r_A + r_X}{\sqrt{2}(r_B + r_X)} \quad (1)$$

where r_A, r_B, and r_X are the ionic radii of the A, B, and X components of the perovskite lattice, respectively. The t can be varied but only in a restrict range of values around the unity, usually between 0.8 and 0.9 for most perovskites, to have a stable, three-dimensional structure with distorted octahedral $[BX_6]$ units. The effective ionic radii of Bi^{3+} and Pb^{2+} ions with a coordination number of VI are 1.03 and 1.19 Å, respectively.[44] For the Bi^{3+} with coordination number XII, which is not listed in Shannon's tables, an ionic radius of 1.36 Å was calculated by extrapolation of Shannon's data for Bi^{3+} ions with lower coordination numbers,[45] which is much smaller than that of $CH_3NH_3^+$ organic cation. As a consequence, doped Bi ions preferentially occupy the Pb site. On the other hand, if Bi ions substitute for $CH_3NH_3^+$, it is anticipated that the telecom emission could also be observed in systems with a similar structure to the $MAPbI_3$. However, control experiment that uses the $MASnI_3$ perovskites as the host of Bi shows the absence of any PL different from its band-edge transition (Figure S7). In addition, it is found that the introduction of Bi into perovskite matrices results in the shift of binding energies of the $4f_{7/2}$ and $4f_{5/2}$ levels of Pb to lower ones, indicating the decreased oxidation states of Pb ions (Figure 2d). All these facts suggest that the BRACs are associated with Pb or $[PbI_6]^-$ octahedra. Although extended X-ray absorption fine structure is a powerful technique to determine the distance, coordination number, and species of the neighbors of the absorbing atom, unfortunately, the overlapping for Bi L_{III} and Pb L_{III} signals makes it extremely hard to gain valuable information.

On the basis of the experimental findings aforementioned, the NIR PL mechanism for Bi-doped $MAPbI_3$ is proposed as follows. Because of the comparable ionic radii of Bi^{3+} and Pb^{2+}, the doped Bi^{3+} ions substitute for the Pb^{2+} ions. As a result, electrons are required to occur to maintain charge neutrality. However, the observation of the spin-paired state indicates the absence of any free electrons. This becomes understandable if two charge-balanced electrons couple with each other through the lattice vibration, forming a singlet bipolaron ($s = 0$) that is doubly charged (Figure 3a). We think that the existence of strong C−H and N−H vibrations in the $MAPbI_3$ matrix renders the coupling of charge-balanced electrons much easier, thus making them ESR-silent. As is well recognized, the

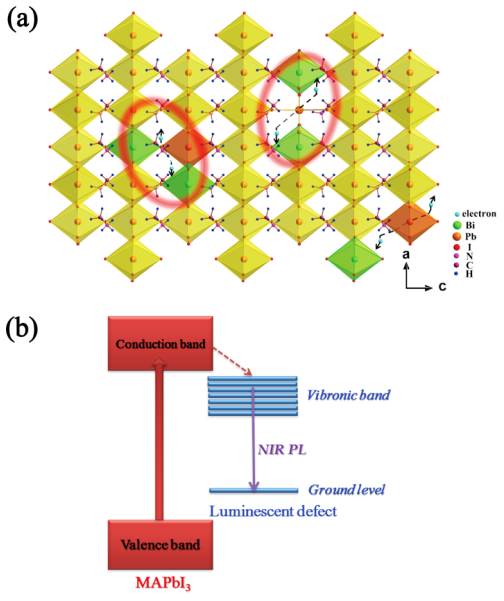

Figure 3. (a) Three-dimensional schematic illustration of the feasible structure of Bi-doped $MAPbI_3$. The units in the red ellipses represent the proposed NIR luminescent centers. (b) Schematic energy diagram of the Bi-doped $MAPbI_3$. The red solid line represents the direct excitation of $MAPbI_3$. The red dotted lines stand for the energy transfer from the $MAPbI_3$ to the luminescent defect, the blue thick lines for the vibronic bands and ground level of the luminescent defect, and the violet solid line for the NIR emission.

DOI: 10.1021/acs.jpclett.6b01147
J. Phys. Chem. Lett. 2016, 7, 2735−2741

presence of the lone pair in the valence shells for some cations such as Pb^{2+} and Bi^{3+} results in the cation being soft,[46] allowing them to adopt states matching the bonding strength of their environments.[47,48] It seems that the valence of Pb is easier to be influenced in comparison to that of Bi (Figure 2c and d), probably due to the larger size of the $[PbI_6]$ octahedron. In view of these, we thus propose that the Bi-doping-induced, distorted $[PbI_6]$ octahedra, coupled with spatially localized bipolarons, form the luminescent center. This center bears the low-energy electronic transition between the vibronic band and ground level, resulting in the ultrawide NIR emission (Figure 3b). That is, the appearance of ultrawide PL in this system results from strong coupling between the BRACs and lattices; the narrowed PL emission at lower temperatures is indicative of the weakened coupling (Figure S8). With increasing Bi concentration, the visible PL, stemming from the $MAPbI_3$, becomes weaker and shorter-lived (Figure 1a and c), owing to the energy transfer to the BRACs and/or nonluminous trapping sites. Time-resolved telecom emission measurements further consolidate that the sensitization of BRACs by the semiconducting matrix. As shown in Figure S9a, for the 0.005% and 0.01% samples, upon nanosecond-pulsed photoexcitation at 2.33 eV, the energy transfer from the matrix to the BRACs dominates; this results that the PL signal reaches the saturation value in a longer duration; however, for the 0.05% and 0.25% samples, because of the increased amount of BRACs, the faster direct excitation of BRACs becomes predominant, followed by energy transfer from the matrix to the BRACs, as reflected by the complex dynamics of their excitation processes. It is also noted that the films with higher Bi concentrations demonstrate relatively shorter lifetimes (Figure S9b), which may be caused by the back energy transfer from the BRACs to the $MAPbI_3$ matrix or concentration quenching.

A notable advantage of lead halide perovskites is that the bandgap tuning can be readily achieved by compositional engineering via simply adjusting the anion or cation species.[6,19] Surprisingly, we find that this technique can be employed as an additional way to rationally tune the photophysical properties of Bi-doped perovskites. As shown in Figure 4a, ultrawide NIR PL with peak wavelengths at 910, 945, and 1100 nm for Bi-doped $MAPbBr_{2.4}Cl_{0.6}$, $MAPbBr_3$, and $MAPbI_{2.4}Br_{0.6}$ films, respectively, can be observed. Given the difference in the lattice parameters of systems investigated here (Figure 4b, Table S2), we could conclude that the lattice expansion of perovskites can result in the red shift of PL from these emitters. Indeed, the BRACs proposed here can be viewed as electrons trapped by the attractive electric field of $[PbX_6]$ polyhedra. Solving for the energy levels of such an electron is a common problem in quantum mechanics; the larger the confinement space, the smaller the absorption and emission energy. Obviously, the lattice expansion from $MAPbBr_{2.4}Cl_{0.6}$ to $MAPbI_3$ is mainly due to the increased size of $[PbX_6]$ polyhedra, which thus, to some extent, justifies the assignment of the BRACs as discussed above.

In order to demonstrate the potential application of the Bi-doped perovskite film in optoelectronic devices, next we fabricated LEDs using it as an emissive layer. The device structure used here is ITO/PEDOT:PSS/$MAPbI_3$:Bi/$PC_{61}BM$/LiF/Al (Figure 5a), where ITO, PEDOT:PSS, and $PC_{61}BM$ represent indium tin oxide, poly(3,4-ethylenedioxythiophene):poly(styrenesulfonate), and [6,6]-phenyl-C61-butyric acid methyl ester, respectively. All layers, with the exception of the electrode, were deposited from

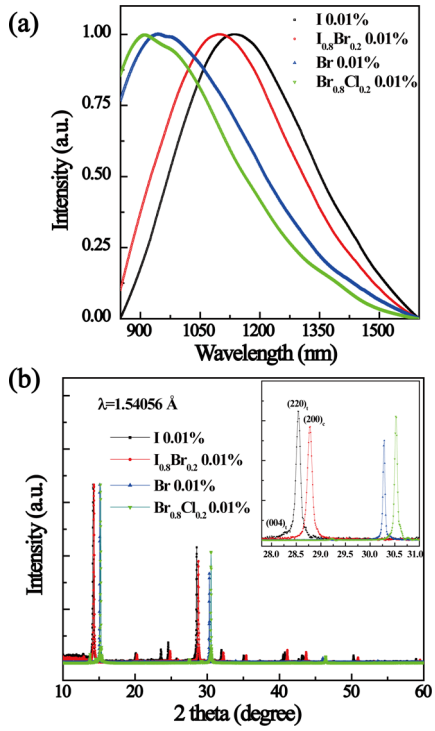

Figure 4. (a) PL spectra of Bi-doped $MAPbBr_{2.4}Cl_{0.6}$ ($Br_{0.8}Cl_{0.2}$), $MAPbBr_3$ (Br), $MAPbI_{2.4}Br_{0.6}$ ($I_{0.8}Br_{0.2}$) and $MAPbI_3$ (I) films under the excitation of 407 nm light. The Bi/Pb molar ratio is 0.01% for all samples. (b) XRD spectra of the Bi-doped $MAPbBr_{2.4}Cl_{0.6}$ ($Br_{0.8}Cl_{0.2}$), $MAPbBr_3$ (Br), $MAPbI_{2.4}Br_{0.6}$ ($I_{0.8}Br_{0.2}$), and $MAPbI_3$ (I) films. The Bi/Pb molar ratio is 0.01% for all samples. Inset shows the enlarged XRD patterns, and characteristic diffraction peaks are indicated.

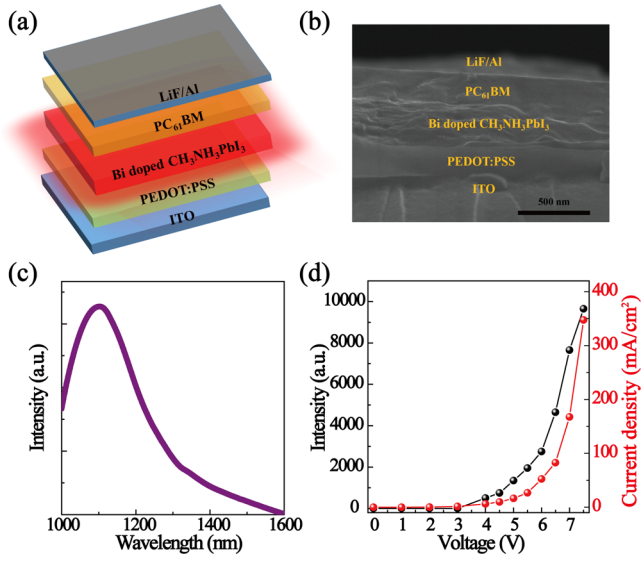

Figure 5. (a) Planar device configuration used for this study. (b) SEM cross-sectional image of the LED. (c) Representative EL spectrum from the LED at an applied voltage of 6 V. The spectral response of the detection system was corrected. (d) Dependence of the current density and EL intensity on the driving voltage.

solution. The corresponding cross-sectional image of the device is presented in Figure 5b. The positions of the valence band maximum and the conduction band minimum of $MAPbI_3$:Bi were determined by the work function according to ultraviolet photoemission spectroscopy (UPS) and the energy gap (Figure

DOI: 10.1021/acs.jpclett.6b01147
J. Phys. Chem. Lett. 2016, 7, 2735−2741

S10, S11). The energy levels of ITO, PEDOT:PSS, $PC_{61}BM$, and LiF/Al were taken from the literature.[11,49,50] Note here we adopted a one-step solution method for nonthermal fabrication of the high-quality Bi-doped perovskite film through the addition of NH_4Cl to the precursor solution,[51] which strongly affects the crystallization process and results in the smooth film with full surface coverage without the need of thermal annealing; it is noteworthy that this film shows slightly blueshifted emission relative to that prepared by the first method (Figure S12). At room temperature, no EL could be measured. However, the EL in the range of 1000−1600 nm, with an fwhm of 226 nm and an emission peak at 1100 nm, is readily observed at 84 K in a device containing a perovskite layer with 0.005% Bi (Figure 5c). Interestingly, the EL is much narrower than the PL (Figure S13), resulting from different excitation mechanisms. The attainment of EL at cryogenic temperatures can be attributed to the increased emission efficiency owing to the suppressed nonradiative channels. At present, it is still hard to measure the external quantum efficiency of the device owing to the experimental difficulties. The current density versus voltage characteristics and the corresponding EL intensity of the device are shown in Figure 5d. A clear turn-on voltage of 4 V was observed. More work is under way in our group to optimize the design of the device for the improvement of its performance.

In summary, we have demonstrated doping of lead halide perovskites can be adopted as a powerful strategy to render this material star luminescent at new wavelengths. Photophysical and structural characterization confirmed that the observed PL originates from one class of Bi-doping-induced optically active center, which is considered to be connected with distorted $[PbI_6]$ units coupled with spatially localized bipolarons. We also found that compositional engineering of these semiconductors can be employed as an additional way to rationally tune the photophysical properties, making them luminesce in a broad spectral range. Finally, we accomplished the electroluminescence at cryogenic temperatures by using Bi-doped $MAPbI_3$ as an emissive layer, marking the first electrically driven devices using Bi-doped photonic materials or lead halide perovskite-based systems containing a small amount of optically active centers. More work will be carried out in the near future to improve thin film quality and PL QEs, as well as optimize device architecture. Beyond our results described above, further investigation into Bi-doped perovskite systems with other compositions is anticipated to help us further increase the PL efficiency and realize room-temperature NIR LEDs. Given the versatility, low-cost processability, and tantalizing emission features, it is envisaged that Bi-functionalized lead halide perovskites may find new applications for optical amplifiers and tunable lasers operating in the telecommunication windows. We anticipate that our present work will stimulate further research to exploit foreign-ion-doped lead halide perovskites and make solution-processable perovskite-based optoelectronic technology even more appealing.

■ ASSOCIATED CONTENT

Supporting Information

The Supporting Information is available free of charge on the ACS Publications website at DOI: 10.1021/acs.jpclett.6b01147.

Experimental details, PL spectra, energy level diagram for the LED, ESR spectra, UPS spectra, the fitted lifetimes, and structural data. (PDF)

■ AUTHOR INFORMATION

Corresponding Authors

*E-mail: timothyhsun@gmail.com (H.-T. Sun).
*E-mail: songbo@suda.edu.cn (B. Song).

Notes

The authors declare no competing financial interest.

■ ACKNOWLEDGMENTS

This work is financially supported by the National Natural Science Foundation of China (Grant Nos. 11574225 and 51472162), Jiangsu Specially Appointed Professor program (Grant No. SR10900214), Natural Science Foundation of Jiangsu Province for Young Scholars (Grant No. BK20140336), Scientific Research Foundation for the Returned Overseas Chinese Scholars, Ministry of Education of China (K510900415), and a project funded by the Priority Academic Program Development of Jiangsu Higher Education Institutions (PAPD).

■ REFERENCES

(1) Kojima, A.; Teshima, K.; Shirai, Y.; Miyasaka, T. Organometal Halide Perovskites as Visible-Light Sensitizers for Photovoltaic Cells. *J. Am. Chem. Soc.* **2009**, *131*, 6050−6051.

(2) Lee, M. M.; Teuscher, J.; Miyasaka, T.; Murakami, T. N.; Snaith, H. J. Efficient Hybrid Solar Cells Based on Meso-Superstructured Organometal Halide Perovskites. *Science* **2012**, *338*, 643−647.

(3) Zhang, W.; Saliba, M.; Moore, D. T.; Pathak, S. K.; Hoerantner, M. T.; Stergiopoulos, T.; Stranks, S. D.; Eperon, G. E.; Alexander-Webber, J. A.; Abate, A.; et al. Ultrasmooth Organic-Inorganic Perovskite Thin-Film Formation and Crystallization for Efficient Planar Heterojunction Solar Cells. *Nat. Commun.* **2015**, *6*, 6142.

(4) Liu, M.; Johnston, M. B.; Snaith, H. J. Efficient Planar Heterojunction Perovskite Solar Cells by Vapour Deposition. *Nature* **2013**, *501*, 395−398.

(5) Xiao, M.; Huang, F.; Huang, W.; Dkhissi, Y.; Zhu, Y.; Etheridge, J.; Gray-Weale, A.; Bach, U.; Cheng, Y.-B.; Spiccia, L. A Fast Deposition-Crystallization Procedure for Highly Efficient Lead Iodide Perovskite Thin-Film Solar Cells. *Angew. Chem., Int. Ed.* **2014**, *53*, 9898−9903.

(6) Pellet, N.; Gao, P.; Gregori, G.; Yang, T.-Y.; Nazeeruddin, M. K.; Maier, J.; Graetzel, M. Mixed-Organic-Cation Perovskite Photovoltaics for Enhanced Solar-Light Harvesting. *Angew. Chem., Int. Ed.* **2014**, *53*, 3151−3157.

(7) Research Cell Efficiency Records. National Renewable Energy Laboratory. http://www.nrel.gov/ncpv (accessed 1 April 2016).

(8) Burschka, J.; Pellet, N.; Moon, S.-J.; Humphry-Baker, R.; Gao, P.; Nazeeruddin, M. K.; Graetzel, M. Sequential Deposition as a Route to High-Performance Perovskite-Sensitized Solar Cells. *Nature* **2013**, *499*, 316−319.

(9) Jeon, N. J.; Noh, J. H.; Yang, W. S.; Kim, Y. C.; Ryu, S.; Seo, J.; Seok, S. I. Compositional Engineering of Perovskite Materials for High-Performance Solar Cells. *Nature* **2015**, *517*, 476−480.

(10) Jeon, N. J.; Noh, J. H.; Kim, Y. C.; Yang, W. S.; Ryu, S.; Il Seok, S. Solvent Engineering for High-Performance Inorganic-Organic Hybrid Perovskite Solar Cells. *Nat. Mater.* **2014**, *13*, 897−903.

(11) Nie, W.; Tsai, H.; Asadpour, R.; Blancon, J.-C.; Neukirch, A. J.; Gupta, G.; Crochet, J. J.; Chhowalla, M.; Tretiak, S.; Alam, M. A.; et al. High-Efficiency Solution-Processed Perovskite Solar Cells with Millimeter-Scale Grains. *Science* **2015**, *347*, 522−525.

(12) Smith, I. C.; Hoke, E. T.; Solis-Ibarra, D.; McGehee, M. D.; Karunadasa, H. I. A Layered Hybrid Perovskite Solar-Cell Absorber with Enhanced Moisture Stability. *Angew. Chem., Int. Ed.* **2014**, *53*, 11232−11235.

(13) Zhou, Z.; Wang, Z.; Zhou, Y.; Pang, S.; Wang, D.; Xu, H.; Liu, Z.; Padture, N. P.; Cui, G. Methylamine-Gas-Induced Defect-Healing

DOI: 10.1021/acs.jpclett.6b01147
J. Phys. Chem. Lett. 2016, 7, 2735−2741

Behavior of CH3NH3PbI3 Thin Films for Perovskite Solar Cells. *Angew. Chem., Int. Ed.* **2015**, *54*, 9705−9709.
(14) Yang, T.-Y.; Gregori, G.; Pellet, N.; Graetzel, M.; Maier, J. The Significance of Ion Conduction in a Hybrid Organic-Inorganic Lead-Iodide-Based Perovskite Photosensitizer. *Angew. Chem., Int. Ed.* **2015**, *54*, 7905−7910.
(15) He, M.; Pang, X.; Liu, X.; Jiang, B.; He, Y.; Snaith, H.; Lin, Z. Monodisperse Dual-Functional Upconversion Nanoparticles Enabled Near-Infrared Organolead Halide Perovskite Solar Cells. *Angew. Chem., Int. Ed.* **2016**, *55*, 4280−4284.
(16) Tan, Z.-K.; Moghaddam, R. S.; Lai, M. L.; Docampo, P.; Higler, R.; Deschler, F.; Price, M.; Sadhanala, A.; Pazos, L. M.; Credgington, D.; et al. Bright Light-Emitting Diodes Based on Organometal Halide Perovskite. *Nat. Nanotechnol.* **2014**, *9*, 687−692.
(17) Jaramillo-Quintero, O. A.; Sanchez, R. S.; Rincon, M.; Mora-Sero, I. Bright Visible-Infrared Light Emitting Diodes Based on Hybrid Halide Perovskite with Spiro-OMeTAD as a Hole-Injecting Layer. *J. Phys. Chem. Lett.* **2015**, *6*, 1883−1890.
(18) Li, G.; Tan, Z.-K.; Di, D.; Lai, M. L.; Jiang, L.; Lim, J. H.-W.; Friend, R. H.; Greenham, N. C. Efficient Light-Emitting Diodes Based on Nanocrystalline Perovskite in a Dielectric Polymer Matrix. *Nano Lett.* **2015**, *15*, 2640−2644.
(19) Sadhanala, A.; Ahmad, S.; Zhao, B.; Giesbrecht, N.; Pearce, P. M.; Deschler, F.; Hoye, R. L. Z.; Goedel, K. C.; Bein, T.; Docampo, P.; et al. Blue-Green Color Tunable Solution Processable Organolead Chloride-Bromide Mixed Halide Perovskites for Optoelectronic Applications. *Nano Lett.* **2015**, *15*, 6095−6101.
(20) Li, J.; Bade, S. G. R.; Shan, X.; Yu, Z. Single-Layer Light-Emitting Diodes Using Organometal Halide Perovskite/Poly(ethylene oxide) Composite Thin Films. *Adv. Mater.* **2015**, *27*, 5196−5202.
(21) Zhang, F.; Zhong, H.; Chen, C.; Wu, X.-g.; Hu, X.; Huang, H.; Han, J.; Zou, B.; Dong, Y. Brightly Luminescent and Color-Tunable Colloidal CH3NH3PbX3 (X = Br, I, Cl) Quantum Dots: Potential Alternatives for Display Technology. *ACS Nano* **2015**, *9*, 4533−4542.
(22) Deschler, F.; Price, M.; Pathak, S.; Klintberg, L. E.; Jarausch, D.-D.; Higler, R.; Huettner, S.; Leijtens, T.; Stranks, S. D.; Snaith, H. J.; et al. High Photoluminescence Efficiency and Optically Pumped Lasing in Solution-Processed Mixed Halide Perovskite Semiconductors. *J. Phys. Chem. Lett.* **2014**, *5*, 1421−1426.
(23) Xing, G.; Mathews, N.; Lim, S. S.; Yantara, N.; Liu, X.; Sabba, D.; Gratzel, M.; Mhaisalkar, S.; Sum, T. C. Low-Temperature Solution-Processed Wavelength-Tunable Perovskites for Lasing. *Nat. Mater.* **2014**, *13*, 476−480.
(24) Zhang, Q.; Ha, S. T.; Liu, X.; Sum, T. C.; Xiong, Q. Room-Temperature Near-Infrared High-Q Perovskite Whispering-Gallery Planar Nano Lasers. *Nano Lett.* **2014**, *14*, 5995−6001.
(25) Zhu, H.; Fu, Y.; Meng, F.; Wu, X.; Gong, Z.; Ding, Q.; Gustafsson, M. V.; Trinh, M. T.; Jin, S.; Zhu, X. Y. Lead Halide Perovskite Nanowire Lasers with Low Lasing Thresholds and High Quality Factors. *Nat. Mater.* **2015**, *14*, 636−642.
(26) Ha, S.-T.; Shen, C.; Zhang, J.; Xiong, Q. Laser Cooling of Organic-Inorganic Lead Halide Perovskites. *Nat. Photonics* **2015**, *10*, 115−121.
(27) Dou, L.; Yang, Y.; You, J.; Hong, Z.; Chang, W.-H.; Li, G.; Yang, Y. Solution-Processed Hybrid Perovskite Photodetectors with High Detectivity. *Nat. Commun.* **2014**, *5*, 5404.
(28) Yakunin, S.; Sytnyk, M.; Kriegner, D.; Shrestha, S.; Richter, M.; Matt, G. J.; Azimi, H.; Brabec, C. J.; Stangl, J.; Kovalenko, M. V.; et al. Detection of X-ray Photons by Solution-Processed Lead Halide Perovskites. *Nat. Photonics* **2015**, *9*, 444−449.
(29) Tian, Y.; Merdasa, A.; Unger, E.; Abdellah, M.; Zheng, K.; McKibbin, S.; Mikkelsen, A.; Pullerits, T.; Yartsev, A.; Sundström, V.; et al. Enhanced Organo-Metal Halide Perovskite Photoluminescence from Nanosized Defect-Free Crystallites and Emitting Sites. *J. Phys. Chem. Lett.* **2015**, *6*, 4171−4177.
(30) Sadhanala, A.; Deschler, F.; Thomas, T. H.; Dutton, S. E.; Goedel, K. C.; Hanusch, F. C.; Lai, M. L.; Steiner, U.; Bein, T.; Docampo, P.; et al. Preparation of Single-Phase Films of $CH_3NH_3Pb(I_{1-x}Br_x)_3$ with Sharp Optical Band Edges. *J. Phys. Chem. Lett.* **2014**, *5*, 2501−2505.
(31) Rehman, W.; Milot, R. L.; Eperon, G. E.; Wehrenfennig, C.; Boland, J. L.; Snaith, H. J.; Johnston, M. B.; Herz, L. M. Charge-Carrier Dynamics and Mobilities in Formamidinium Lead Mixed-Halide Perovskites. *Adv. Mater.* **2015**, *27*, 7938−7944.
(32) Sutherland, B. R.; Sargent, E. H. Perovskite Photonic Sources. *Nat. Photonics* **2016**, *10*, 295−302.
(33) Ning, Z.; Gong, X.; Comin, R.; Walters, G.; Fan, F.; Voznyy, O.; Yassitepe, E.; Buin, A.; Hoogland, S.; Sargent, E. H. Quantum-Dot-in-Perovskite Solids. *Nature* **2015**, *523*, 324−328.
(34) Stranks, S. D.; Snaith, H. J. Metal-Halide Perovskites for Photovoltaic and Light-Emitting Devices. *Nat. Nanotechnol.* **2015**, *10*, 391−402.
(35) Sanchez, R. S.; de la Fuente, M. S.; Suarez, I.; Munoz-Matutano, G.; Martinez-Pastor, J. P.; Mora-Sero, I. Tunable light emission by exciplex state formation between hybrid halide perovskite and core/shell quantum dots: Implications in advanced LEDs and photovoltaics. *Sci. Adv.* **2016**, *2*, e1501104.
(36) Mocatta, D.; Cohen, G.; Schattner, J.; Millo, O.; Rabani, E.; Banin, U. Heavily Doped Semiconductor Nanocrystal Quantum Dots. *Science* **2011**, *332*, 77−81.
(37) Zhou, Y.; Zhou, D.-D.; Liu, B.-M.; Li, L.-N.; Yong, Z.-J.; Xing, H.; Fang, Y.-Z.; Hou, J.-S.; Sun, H.-T. Ultrabroad Near-Infrared Photoluminescence from Bismuth Doped $CsPbI_3$: Polaronic Defects vs. Bismuth Active Centers. *J. Mater. Chem. C* **2016**, *4*, 2295−2301.
(38) Sun, H.-T.; Zhou, J.; Qiu, J. Recent Advances in Bismuth Activated Photonic Materials. *Prog. Mater. Sci.* **2014**, *64*, 1−72.
(39) Liu, B.-M.; Zhang, Z.-G.; Zhang, K.; Kuroiwa, Y.; Moriyoshi, C.; Yu, H.-M.; Li, C.; Zheng, L.-R.; Li, L.-N.; Yang, G.; et al. Unconventional Luminescent Centers in Metastable Phases Created by Topochemical Reduction Reactions. *Angew. Chem., Int. Ed.* **2016**, *55*, 4967−4971.
(40) de Jong, M.; Meijerink, A.; Barandiaran, Z.; Seijo, L. Structure and Hindered Vibration of Bi^{2+} in the Red-Orange Phosphor SrB_4O_7:Bi. *J. Phys. Chem. C* **2014**, *118*, 17932−17939.
(41) Toma, O.; Allain, M.; Meinardi, F.; Forni, A.; Botta, C.; Mercier, N. Bismuth-Based Coordination Polymers with Efficient Aggregation-Induced Phosphorescence and Reversible Mechanochromic Luminescence. *Angew. Chem., Int. Ed.* **2016**, *55*, 7998.
(42) Fang, H.-H.; Raissa, R.; Abdu-Aguye, M.; Adjokatse, S.; Blake, G. R.; Even, J.; Loi, M. A. Photophysics of Organic-Inorganic Hybrid Lead Iodide Perovskite Single Crystals. *Adv. Funct. Mater.* **2015**, *25*, 2378−2385.
(43) Poglitsch, A.; Weber, D. Dynamic Disorder in Methylammoniumtrihalogenoplumbates(II) Observed by Millimeter-Wave Spectroscopy. *J. Chem. Phys.* **1987**, *87*, 6373−6378.
(44) Shannon, R. D. Revised Effective Ionic-Radii and Systematic Studies of Interatomic Distances in Halides and Chalcogenides. *Acta Crystallogr., Sect. A: Cryst. Phys., Diffr., Theor. Gen. Crystallogr.* **1976**, *32*, 751−767.
(45) Suchomel, M. R.; Davies, P. K. Predicting the Position of the Morphotropic Phase Boundary in High Temperature $PbTiO_3$-$Bi((BB')$-$B-')O_3$ Based Dielectric Ceramics. *J. Appl. Phys.* **2004**, *96*, 4405−4410.
(46) Brown, I. D. Recent Developments in the Methods and Applications of the Bond Valence Model. *Chem. Rev.* **2009**, *109*, 6858−6919.
(47) Groenink, J. A.; Blasse, G. Some New Observations on the Luminescence of Pbmoo4 and Pbwo4. *J. Solid State Chem.* **1980**, *32*, 9−20.
(48) Babin, V.; Oskam, K. D.; Vergeer, P.; Meijerink, A. The Role of Pb^{2+} as a Sensitizer for Gd^{3+}-Eu^{3+} Downconversion Couple in Fluorides. *Radiat. Meas.* **2004**, *38*, 767−770.
(49) Seo, J.; Park, S.; Kim, Y. C.; Jeon, N. J.; Noh, J. H.; Yoon, S. C.; Seok, S. I. Benefits of very Thin PCBM and LiF Layers for Solution-Processed P-I-N Perovskite Solar Cells. *Energy Environ. Sci.* **2014**, *7*, 2642−2646.

DOI: 10.1021/acs.jpclett.6b01147
J. Phys. Chem. Lett. 2016, 7, 2735−2741

(50) Wang, J.; Wang, N.; Jin, Y.; Si, J.; Tan, Z.-K.; Du, H.; Cheng, L.; Dai, X.; Bai, S.; He, H.; et al. Interfacial Control Toward Efficient and Low-Voltage Perovskite Light-Emitting Diodes. *Adv. Mater.* **2015**, *27*, 2311−2316.
(51) Chen, Y.; Zhao, Y.; Liang, Z. Non-Thermal Annealing Fabrication of Efficient Planar Perovskite Solar Cells with Inclusion of NH_4Cl. *Chem. Mater.* **2015**, *27*, 1448−1451.

DOI: 10.1021/acs.jpclett.6b01147
J. Phys. Chem. Lett. 2016, 7, 2735−2741